Partial volume segmentation of brain magnetic resonance images based on maximum *a posteriori* probability

Xiang Li[a)]
Department of Radiology, State University of New York at Stony Brook, Stony Brook, New York, 11794 and Department of Radiation Oncology, Columbia University, New York, New York, 10032

Lihong Li
Department of Radiology, State University of New York at Stony Brook, Stony Brook, New York, 11794 and Department of Engineering Science and Physics, College of Staten Island of the City University of New York, Staten Island, New York 10314

Hongbing Lu
Department of Radiology, State University of New York at Stony Brook, Stony Brook, New York 11794 and Department of Biomedical Engineering/Computer Application, Fourth Military Medical University, Xi'an, Shaanxi 710032, China

Zhengrong Liang
Department of Radiology, State University of New York at Stony Brook, Stony Brook, New York 11794

(Received 23 September 2004; revised 9 May 2005; accepted for publication 9 May 2005; published 22 June 2005)

Noise, partial volume (PV) effect, and image-intensity inhomogeneity render a challenging task for segmentation of brain magnetic resonance (MR) images. Most of the current MR image segmentation methods focus on only one or two of the above-mentioned effects. The objective of this paper is to propose a unified framework, based on the maximum *a posteriori* probability principle, by taking all these effects into account simultaneously in order to improve image segmentation performance. Instead of labeling each image voxel with a unique tissue type, the percentage of each voxel belonging to different tissues, which we call a mixture, is considered to address the PV effect. A Markov random field model is used to describe the noise effect by considering the nearby spatial information of the tissue mixture. The inhomogeneity effect is modeled as a bias field characterized by a zero mean Gaussian prior probability. The well-known fuzzy C-mean model is extended to define the likelihood function of the observed image. This framework reduces theoretically, under some assumptions, to the adaptive fuzzy C-mean (AFCM) algorithm proposed by Pham and Prince. Digital phantom and real clinical MR images were used to test the proposed framework. Improved performance over the AFCM algorithm was observed in a clinical environment where the inhomogeneity, noise level, and PV effect are commonly encountered. © *2005 American Association of Physicists in Medicine*. [DOI: 10.1118/1.1944912]

Key words: magnetic resonance imaging, fuzzy C-mean algorithm, Markov random field, PV segmentation, intensity inhomogeneity correction

I. INTRODUCTION

Magnetic resonance (MR) imaging has several advantages over other medical imaging modalities, including high contrast among different soft tissues, relatively high spatial resolution across the entire field of view (FOV), and multispectral characteristics. Therefore, it has been widely used in quantitative brain imaging studies. Quantitative volumetric measurement and three-dimensional (3D) visualization of brain tissues are helpful for pathological evolution analyses, where image segmentation plays an important role. Incorporating multispectral analysis into MR image segmentation was pioneered by Vannier *et al.*[1] and has been widely adopted by other researchers.

Noise, partial volume (PV) effect, and image-intensity inhomogeneity across the FOV render a challenging task for MR image segmentation. Currently, the majority of brain MR image segmentation algorithms focus on one or two of the above listed effects. A variety of intensity-based segmentation methods[2–5] has been proposed and achieved notable success in the absence of inhomogeneity and PV effects. These methods model the image intensity distribution as a multivariate likelihood function and apply the Markov random field (MRF) theory to specify the *prior* probability of the tissue type distribution, resulting in a robust maximum *a posteriori* (MAP) probability image segmentation in the presence of noise. However, these methods belong to the category of hard segmentation, in which each voxel is classified as a single tissue type. Due to the limited spatial resolution of most imaging devices and complex anatomical structure of the brain tissues, there are often some voxels in the images that contain two or more tissue types. In other words, PV effect is rather common. Currently, there are two popular PV models: the fuzzy C-mean (FCM)[6–9] and the Gaussian distribution[10–12] models.

Due to the nonuniformity in the rf field during data acquisition,[13,14] the inhomogeneity effect usually results in a

shading effect across the whole MR image. Current methods of correcting for this effect can be divided into two categories. The first category is called the straightforward approach. For example, Dawant *et al.*[15] manually selected some reference points within the image, and then reconstructed the bias field with a spline surface fitting technique. Some researchers[16–19] have adopted the homomorphic filter to correct for the inhomogeneity effect. Volurka *et al.*[20] used the local gradient information in the image to estimate the bias field. Lee and Vannier[21] proposed an extended FCM clustering algorithm to reconstruct the bias field. Chen *et al.*[22] applied the group theory to extract the lowest-frequency component of the image for the bias field. The second category corrects for the inhomogeneity effect during image segmentation and is called the simultaneous approach. Wells *et al.*[23] proposed a MAP estimation of the bias field, in which an estimation of the *posteriori* probability of voxel labels was produced as a side-effect. Guillemaud and Brady[24] further refined this method by introducing an extra class for the bias field. More studies on the method were performed subsequently by Held *et al.*[25] and Kapur and Pohl,[26,27] where a MRF modeling for noise reduction was added. The approach of Held *et al.* moved to hard labeling via the iterated conditional modes (ICM) approach, while Kapur and Pohl remained in the soft labeling domain by estimating the *posteriori* probability of voxel labels using the mean-field approach. Pham *et al.*[6,7] proposed an unsupervised method, called the adaptive fuzzy C-mean (AFCM) algorithm, which can correct for the inhomogeneity effect and segment directly the tissue partial volumes (not the *posteriori* probability of the voxel labels) in each image voxel simultaneously. It performs very well under low noise conditions. However, its performance deteriorates quickly as the noise goes up, because it does not incorporate a MRF model to control the noise.

The objective of this paper is to propose a unified framework to improve brain MR image segmentation by considering all effects simultaneously using the MAP probability principle.

II. THEORY

A. PV-MAP framework

Let image intensities Y be a column vector $[y_1, y_2, \ldots, y_N]^T$, where N is the total number of image voxels in an acquired image. For multispectral imaging, y_i becomes a vector $[y_{i1}, y_{i2}, \ldots, y_{iL}]^T$, where L represents the total number of multispectral MR images. Let mixture M be a vector $[m_1, m_2, \ldots, m_N]^T$ with the following properties: (1) $m_i = [m_{i1}, m_{i2}, \ldots, m_{iK}]^T$, and (2) $\Sigma_{k=1}^{K} m_{ik} = 1$, $0 \leqslant m_{ik} \leqslant 1$, where m_{ik} reflects the fraction of issue type k inside voxel i, which is called a mixture, and K is the total number of tissue classes in the multispectral MR images. Let bias field $B = [\beta_1, \beta_2, \ldots, \beta_N]^T$ be the shading effect across the whole FOV, where β_i is a vector $[\beta_{i1}, \beta_{i2}, \ldots, \beta_{iL}]^T$ for multispectral imaging. Let Φ be a parameter set, which depends on the model of the observed images Y.

According to the MAP principle, estimation of the mixture M, bias field B, and tissue class parameter set Φ, given observed images Y, can be performed by maximizing the posterior distribution:

$$P(M,B,\Phi|Y) = \frac{P(Y|M,B,\Phi)P(M,B,\Phi)}{P(Y)} \propto P(Y|M,B,\Phi)P(M,B,\Phi). \quad (1)$$

Assuming the mixture M, bias field B, and parameter Φ are independent, we have

$$P(M,B,\Phi|Y) \propto P(Y|M,B,\Phi)P(M|B,\Phi)P(B|\Phi)P(\Phi) = P(Y|M,B,\Phi)P(M)P(B)P(\Phi). \quad (2)$$

By logarithmic transformation, Eq. (2) becomes

$$-\ln P(M,B,\Phi|Y) \propto U(Y|M,B,\Phi) + U(M) + U(B) + U(\Phi), \quad (3)$$

where $U(Y|M,B,\Phi)$ is the likelihood energy function of the observed images Y, and $U(M), U(B)$, and $U(\Phi)$ are the prior energy functions of the mixture M, the bias field B, and the parameter set Φ, respectively.

The following definition is chosen for the likelihood energy function of the observed images Y:

$$U(Y|M,B,\Phi) = \sum_{j=1}^{L}\sum_{i=1}^{N}\sum_{k=1}^{K} m_{ik}^2 \|y_{ij} - \beta_{ij} \cdot \upsilon_{jk}\|^2, \quad (4)$$

where υ_{jk} is the centroid of tissue class k in multispectral MR image j. Notation $\| \|^2$ represents the Euclidean norm. This cluster model for tissue mixture m_{ik} in multispectral MR images Y has been used by other researchers[6–8] and our group.[9] Without the bias field term β_{ij}, Eq. (4) reduces to the standard FCM model.[6–8] In this study, Φ is defined as a set $\{\upsilon_{jk}; 1 \leqslant j \leqslant L, 1 \leqslant k \leqslant K\}$.

A MRF model is applied to define the prior distribution of mixture M:

$$P(M) = \frac{1}{Z}\exp\left(-\alpha\sum_{i=1}^{N}\sum_{k=1}^{K}\sum_{r\in N_i}\kappa_r\|m_{ik} - m_{rk}\|^2\right), \quad (5)$$

where N_i denotes the neighborhood of image voxel i, α is a parameter controlling the degree of the smooth penalty on the mixture M, κ_r is a scaling factor reflecting the difference among different orders of neighbors, and Z is the normalization factor for the MRF model. In this study, only the first-order neighborhood system was considered. Thus, the prior energy function for the mixture model can be expressed as

$$U(M) = \alpha\sum_{i=1}^{N}\sum_{k=1}^{K}\sum_{r\in N_i}\kappa_r\|m_{ik} - m_{rk}\|^2. \quad (6)$$

The bias field B is modeled by a zero mean Gaussian prior probability density of

$$P(B) = (2\pi)^{-N/2}|\Sigma_B|^{-1/2}\exp\left(-\frac{1}{2}B^T\Sigma_B B\right). \quad (7)$$

Usually the covariance matrix Σ_B is too large to manipulate. In order to simplify the calculation, Wells *et al.*[23] proposed that Σ_B might be chosen to be a banded matrix, which represents a low-pass filter. We adopted this strategy in this study. Therefore, the prior energy function of the bias field B is described by

$$U(B) = \tfrac{1}{2}B^T\Sigma_B B. \quad (8)$$

The penalty term on the bias field proposed in Pham and Prince's papers[6,7] can be regarded as a special choice of the covariance matrix Σ_B in Eq. (8). Here, we adopted the definition of Σ_B from Pham and Prince's papers as

$$U(B) = \lambda_1\sum_{j=1}^{L}\sum_{i=1}^{N}\sum_{l=1}^{R}(D_l{}^*B_j)_i^2 + \lambda_2\sum_{j=1}^{L}\sum_{i=1}^{N}\sum_{l=1}^{R}\sum_{h=1}^{R}(D_l{}^*D_h{}^*B_j)_i^2, \quad (9)$$

where R equals two for two-dimensional situations or three for 3D applications. $B_j=[\beta_{1j},\beta_{2j},\beta_{Nj}]^T$ is the bias field of MR image j. Notation D is the standard forward finite difference operator along the corresponding directions. The asterisk denotes the one-dimensional (1D) discrete convolution operator. The first-order regularization term (associated with λ_1) penalizes a large variation in the bias field and the second-order regularization term (associated with λ_2) penalizes the discontinuities in the bias field. Parameters λ_1 and λ_2 control the degree of smoothness of the bias field.

The parameter set Φ is modeled as a uniform distribution for all tissue classes in this paper, thus the prior energy function of Φ is a constant. Therefore, according to the above-given definitions, we have the posterior energy function:

$$U = \sum_{j=1}^{L}\sum_{i=1}^{N}\sum_{k=1}^{K} m_{ik}^2\|y_{ij}-\beta_{ij}\cdot\upsilon_{jk}\|^2 + \alpha\sum_{i=1}^{N}\sum_{k=1}^{K}\sum_{r\in N_i}\kappa_r\|m_{ik}-m_{rk}\|^2 + \lambda_1\sum_{j=1}^{L}\sum_{i=1}^{N}\sum_{l=1}^{R}(D_l{}^*B_j)_i^2 + \lambda_2\sum_{j=1}^{L}\sum_{i=1}^{N}\sum_{l=1}^{R}\sum_{h=1}^{R}(D_l{}^*D_h{}^*B_j)_i^2, \quad (10)$$

where the asterisk was defined before as the 1D discrete convolution operator.

Given the posterior energy function, our next task is to minimize the function for estimations of the mixture M, bias field B, and parameter set Φ.

B. Segmentation of tissue mixtures

In searching for a solution to minimize the posterior energy function (10) with respect to mixture M, an ICM-like algorithm was utilized in this study. It is noted that solving the exact optimization as formulated in Eq. (10) is computationally impracticable. In order to achieve computational efficiency, we adopted the ICM-like approach, which utilizes the iterative local minimization. Their convergence is guaranteed after only a few iterations. Equivalently, the solution is determined by maximizing the posterior energy function of

$$U = \sum_{j=1}^{L}\sum_{i=1}^{N}\sum_{k=1}^{K} m_{ik}^2\|y_{ij}-\beta_{ij}\cdot\upsilon_{jk}\|^2 + \alpha\sum_{i=1}^{N}\sum_{k=1}^{K}\sum_{r\in N_i}\kappa_r\|m_{ik}-m_{rk}\|^2 + \sum_{i=1}^{N}\gamma_i\left(1-\sum_{k=1}^{K}m_{ik}\right) \quad (11)$$

under the condition of $\Sigma_{k=1}^{K} m_{ik}=1$, where γ_i is the Lagrange multiplier, and the two terms associated with λ_1 and λ_2 are omitted because they are parameters of bias field B and independent from mixture M.

Taking the partial derivative with respect to the mixture m_{ik} and setting it to zero, we have

$$m_{ik}^{(n+1)} = \frac{\gamma_i + 4\alpha\Sigma_{r\in N_i}\kappa_r m_{rk}^{(n)}}{2\Sigma_{j=1}^{L}\|y_{ij}-\beta_{ij}\cdot\upsilon_{jk}\|^2 + 4\alpha\Sigma_{r\in N_i}\kappa_r}. \quad (12)$$

By the constraint of $\Sigma_{k=1}^{K} m_{ik}=1$ for every i, γ_i can be calculated by substituting m_{ik} into this constraint and is given by

$$\gamma_i = \frac{1-\Sigma_{k=1}^{K}\dfrac{4\alpha\Sigma_{r\in N_i}\kappa_r m_{rk}^{(n)}}{2\Sigma_{j=1}^{L}\|y_{ij}-\beta_{ij}\upsilon_{jk}\|^2 + 4\alpha\Sigma_{r\in N_i}\kappa_r}}{\Sigma_{k=1}^{K}\dfrac{1}{2\Sigma_{j=1}^{L}\|y_{ij}-\beta_{ij}\upsilon_{jk}\|^2 + 4\alpha\Sigma_{r\in N_i}\kappa_r}}. \quad (13)$$

Substituting γ_i back into Eq. (12) results in the estimation of mixture m_{ik} or segmentation of tissue mixtures by

$$m_{ik}^{(n+1)} = \frac{1-\Sigma_{l=1}^{K}\dfrac{4\alpha\Sigma_{r\in N_i}\kappa_r(m_{rl}^{(n)}-m_{rk}^{(n)})}{2\Sigma_{j=1}^{L}\|y_{ij}-\beta_{ij}\upsilon_{jl}\|^2 + 4\alpha\Sigma_{r\in N_i}\kappa_r}}{\Sigma_{l=1}^{K}\dfrac{2\Sigma_{j=1}^{L}\|y_{ij}-\beta_{ij}\cdot\upsilon_{jk}\|^2 + 4\alpha\Sigma_{r\in N_i}\kappa_r}{2\Sigma_{j=1}^{L}\|y_{ij}-\beta_{ij}\upsilon_{jl}\|^2 + 4\alpha\Sigma_{r\in N_i}\kappa_r}}. \quad (14)$$

Leemput *et al.*[11] suggested that prior constraints on the mixture with $\Sigma_{k=1}^{K} m_{ik}=1$, $0\leqslant m_{ik}\leqslant 1$ is too loose for brain MR image segmentation. They assumed that there are at most two tissue types inside each voxel: gray matter (GM) and white matter (WM) or gray matter and cerebrospinal fluid (CSF). In addition, they used a down-sampling process to model the PV effect so that mixture m_{ik} is restricted to be discrete values. Therefore, their solution set can be defined as follows: (1) $m_{i\mathrm{GM}}+m_{i\mathrm{WM}}=1$ and $m_{i\mathrm{CSF}}=0$, or (2) $m_{i\mathrm{GM}}+m_{i\mathrm{CSF}}=1$ and $m_{i\mathrm{WM}}=0$; where $m_{ik}\in\{0,1/J,2/J,,(J-1)/J,1\}$ and J is the number of subvoxels per image voxel. In this paper, we applied the same prior constraint of $\Sigma_{k=1}^{K} m_{ik}=1$. Since the energy function defined in Eq. (11) is quadratic with respect to m_{ik}, our MAP approach based on this more restrictive prior knowledge seeks a solution, which has the smallest distance from the solutions determined by Eq. (14).

C. Estimation of bias field

Taking the first partial derivative of the objective function U in Eq. (10) with respect to the bias field β_{ij} and setting it to zero shall result in

$$-\sum_{k=1}^{K} m_{ik}^2 v_{jk}(y_{ij}-\beta_{ij}v_{jk})+\lambda_1(H_1{}^{**}B_j)_i+\lambda_2(H_2{}^{**}B_j)_i=0, \tag{15}$$

where two asterisks denote the 2D discrete convolution operator. We have adopted the same matrices H_1 and H_2 from Pham's papers, which are defined as follows for the 2D situation (for the 3D situation, it becomes more complicated as seen in Ref. 7):

$$H_1=\begin{bmatrix} 0 & -1 & 0 \\ -1 & 4 & -1 \\ 0 & -1 & 0 \end{bmatrix}, \quad H_2=\begin{bmatrix} 0 & 0 & 1 & 0 & 0 \\ 0 & 2 & -8 & 2 & 0 \\ 1 & -8 & 20 & -8 & 1 \\ 0 & 2 & -8 & 2 & 0 \\ 0 & 0 & 1 & 0 & 0 \end{bmatrix}. \tag{16}$$

Rearranging this equation, we obtain

$$\sum_{k=1}^{K} v_{jk}y_{ij}m_{ik}^2=\beta_{ij}\cdot\sum_{k=1}^{K} v_{jk}^2 m_{ik}^2+\lambda_1(H_1{}^{**}B_j)_i+\lambda_2(H_2{}^{**}B_j)_i. \tag{17}$$

It is difficult to calculate the bias field B directly from Eq. (17). To mitigate this difficulty, the Jacobi iterative scheme[28] was employed to solve this equation. A brief review of the Jacobi iterative scheme is given below. Equation (17) can be rewritten in terms of matrix:

$$Q=WB_j+(\lambda_1C_1+\lambda_2C_2)B_j=(W+C)B_j=AB_j, \tag{18}$$

where Q is a vector with elements $\Sigma_{k=1}^{K} v_{jk}y_{ij}m_{ik}^2$, and W is a diagonal matrix with elements $\Sigma_{k=1}^{K} v_{jk}^2 m_{ik}^2$. C_1B_j and C_2B_j are matrix expressions of $H_1{}^{**}B_j$ and $H_2{}^{**}B_j$, respectively, and $A=W+C=W+\lambda_1C_1+\lambda_2C_2$.

If matrix A is decomposed such that $A=E-F-G$, where E,F,G are the diagonal, lower triangular, and upper triangular matrices, respectively, the bias field B can be solved by the Jacobi iterative scheme:

$$B_j^{(m+1)}=[(1-\omega)I+\omega E^{-1}(F+G)]B_j^{(m)}+\omega E^{-1}Q, \tag{19}$$

where ω is a weighting parameter and I is the identity matrix.

In general, at least several hundred (the number of image array dimensions) iterations are needed to achieve convergence, which is very time consuming. The multigrid strategy[27] provides a way to reduce the computing effort and was used in this study. A detailed description of the multigrid algorithm can be found in the literature.[6,7,29]

D. Estimation of centroid for each tissue class

In a similar way, taking the first partial derivative of the objective function U in Eq. (10) with respect to the centroid v_{jk} of class k from image j and setting it to zero shall lead to

$$\sum_{i=1}^{N} m_{ik}^2\beta_{ij}(y_{ij}-\beta_{ij}\cdot v_{jk})=0. \tag{20}$$

By rearranging Eq. (20), we have

$$v_{jk}=\frac{\Sigma_{i=1}^{N} m_{ik}^2\beta_{ij}y_{ij}}{\Sigma_{i=1}^{N} m_{ik}^2\beta_{ij}^2}. \tag{21}$$

E. Summary of the PV-MAP segmentation/estimation algorithm

The presented brain MR image segmentation algorithm, which simultaneously takes into account the multispectral nature, noise, PV effect, and image inhomogeneity, can be summarized as follows:

(1) Set the initial bias field $\{\beta_{ij}\}_{i=1}^{N}$ equal to one for all voxels and estimate the initial value of centroid v_{jk} for each tissue class and the initial membership m_{ik}. Here, we adopted the self-adaptive vector quantization method[30] to automatically set the initial centroid v_{jk} and the associated hard segmentation. The hard segmentation result can be easily transferred into mixture m_{ik} by setting it to 1 if k equals the label value of voxel i. Otherwise, m_{ik} shall be zero.
(2) Perform PV segmentation for mixture m_{ik} using Eq. (14).
(3) Update the bias field using the Jacobi iterative scheme with the multigrid method by Eq. (19).
(4) Compute the new centroids v_{jk} for each tissue class using Eq. (21).
(5) If the iterative process satisfies the termination criterion of Eq. (22), the updated mixture $\{m_{ik}\}$ and bias field $\{\beta_{ij}\}_{i=1}^{N}$ are saved as the final results. Otherwise, go to step 2.

An empirical, yet commonly used criterion for terminating iterative process is written as

$$\max\left(\left|\frac{v_{jk}^{(n+1)}}{v_{jk}^{(n)}}-1\right|\right)\leqslant\epsilon. \tag{22}$$

When the difference between the centroid v_{jk} of each class at the $(n+1)$-th iteration and at the nth iteration is less than the threshold ϵ as specified by the user, the iterative process terminates. In this study, the threshold ϵ was set to be 0.01.

III. RESULTS

The presented PV-MAP method was tested using both digital phantom and clinical MR images and compared with the conventional FCM and AFCM algorithms. In the quantitative comparison, the following measures were used: the

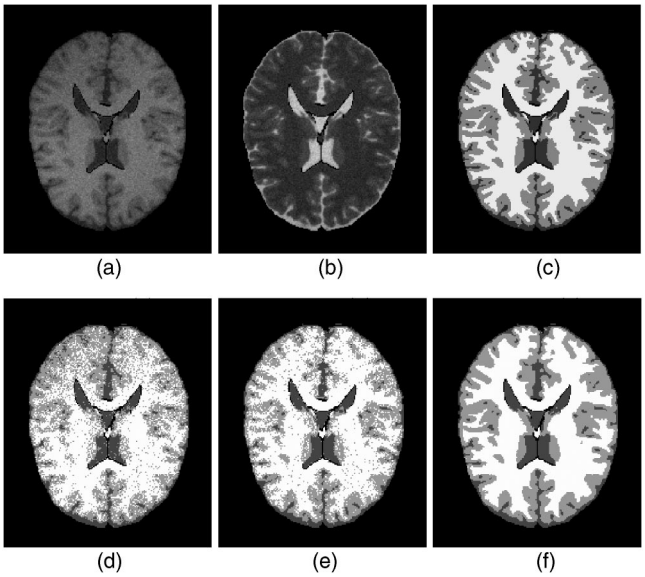

FIG. 1. Digital phantom studies. (a) T_1 weighted image. (b) T_2 weighted image. (c) The ground truth of hard segmentation. (d) The FCM segmentation. (e) The AFCM segmentation. (f) The presented PV-MAP segmentation.

true positive fraction (TPF), the false positive fraction (FPF), and the accurate segmentation ratio (ASR), which are described as

$$\mathrm{TPF} = \frac{\mathrm{Volume}^{+}_{\mathrm{seg}} \cap \mathrm{Volume}^{+}_{\mathrm{true}}}{\mathrm{Volume}^{+}_{\mathrm{true}}} \times 100\,\%\,,$$

$$\mathrm{FPF} = \frac{\mathrm{Volume}^{-}_{\mathrm{seg}} \cap \mathrm{Volume}^{+}_{\mathrm{true}}}{\mathrm{Volume}^{+}_{\mathrm{true}}} \times 100\,\%\,, \tag{23}$$

$$\mathrm{ASR} = \frac{\text{whole volume}^{+}_{\mathrm{seg}} \cap \text{whole volume}^{+}_{\mathrm{true}}}{\text{whole volume}^{+}_{\mathrm{true}}} \times 100\%$$

where a + or − sign represents whether a voxel is or is not of a specific tissue type. TPF and FPF are used to measure the performance of different algorithms for a specific tissue, and ASR provides the overall evaluation based on the entire image volume. Obviously, a perfect segmentation has a TPF equal to one, FPF of zero, and ASR of one.

A. Digital phantom studies

The digital brain phantoms obtained from McConnell Brain Imaging Center of the Montreal Neurological Institute were used to evaluate our method.[31] For this study, we downloaded the 3D T_1 and T_2 phantom images with 5% noise and 60% inhomogeneity effect. Figures 1(a) and 1(b) show the single slice T_1 and T_2 weighted images, respectively.

Figure 1(c) is the ground truth of hard segmentation. The PV segmentation results of different algorithms were obtained first and then converted into hard segmentations, respectively, for comparison purpose. The conversion labels a voxel by a tissue type, which has the largest mixture percentage among all the tissue types in that voxel. Figure 1(d) is the hard segmentation converted from the FCM segmentation result. Because of the inhomogeneity effect, the WM is missed at the top region and oversegmented at the bottom area. Figures 1(e) and 1(f) show the hard segmentation results converted from the AFCM and our PV-MAP segmentations, respectively. Both methods can correct for the inhomogeneity effect very well. However, there are many speckles in the AFCM segmentation due to the presence of noise. By visual judgment, our method has a better performance against noise compared with the AFCM result. For a more objective comparison among the FCM, AFCM, and our method, a quantitative analysis of the whole 3D image volume was conducted. Table I shows the quantitative results of different methods based on the TPF, FPF, and ASR measures. In the presence of noise and the inhomogeneity effect, the ASR value of the FCM algorithm is very low (75.16%), which is not acceptable in the clinic. Because the AFCM algorithm takes into account the inhomogeneity effect, its ASR value can be improved to 82.60%. An improvement in TPF and FPF is also noticeable. It is notable that the presented method can achieve an ASR value of 91.49% and improve TPF and FPF for all tissue types.

Figure 2 shows the segmented mixture images of different tissue types obtained using different segmentation methods. Figures 2(a)–2(c) are the true mixture models of CSF, GM, and WM, respectively. Figures 2(d)–2(f) show the mixture images of CSF, GM, and WM obtained with the FCM algorithm. It is noted that there are severe shading artifacts on the GM and WM mixtures because the FCM did not correct for the image intensity inhomogeneity. This shading effect is completely removed by the AFCM and PV-MAP method, as shown in Figs. 2(g)–2(l). However, segmented mixture images obtained via the AFCM method demonstrate a weak performance against noise. By including the MRF model into the presented PV-MAP framework, our segmentation scheme overcomes not only the inhomogeneity effect but also the noise effect.

The presented PV-MAP method has three parameters, α, λ_1, and λ_2, to be specified, as shown in Eq. (10). For a penalized estimation algorithm, the robustness of these pa-

TABLE I. Quantitative comparison of FCM, AFCM, and PV-MAP methods (%).

	FCM			AFCM			PV-MAP		
	WM	GM	CSF	WM	GM	CSF	WM	GM	CSF
TPF	74.57	73.60	80.69	76.58	85.80	93.26	91.96	90.27	93.96
FPF	21.42	31.66	15.63	7.58	31.08	12.95	6.94	9.08	10.92
ASR		75.16			82.60			91.49	

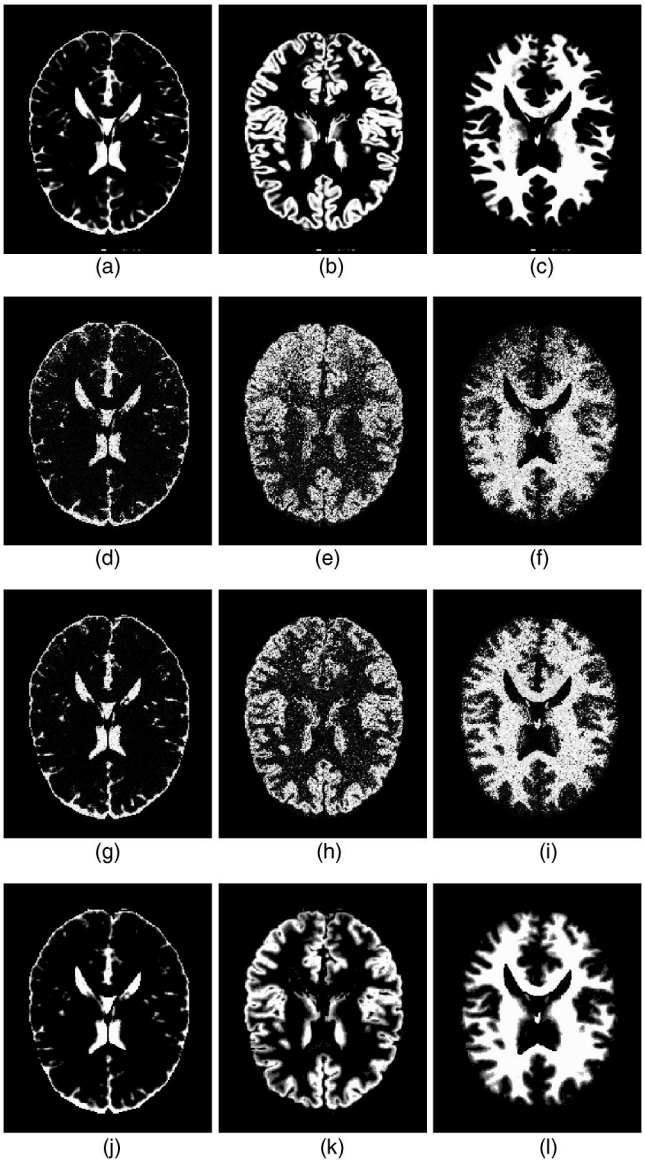

FIG. 2. Comparison on segmented mixture images. (a) The true model of CSF mixture. (b) The true model of GM mixture. (c) The true model of WM mixture. (d) The segmented CSF mixture by FCM. (e) The segmented GM mixture by FCM. (f) The segmented WM mixture by FCM. (g) The CSF mixture by AFCM. (h) The GM mixture by AFCM. (i) The WM mixture by AFCM. (j) The CSF mixture of PV-MAP. (k) The GM mixture of PV-MAP. (l) The WM mixture of PV-MAP.

rameters is a very important issue. In Ref. 7, the robustness of parameters λ_1 and λ_2 has been studied. Based on that work,[7] λ_1 and λ_2 were determined to be 40 000 and 400 000, respectively. The value of parameter α is empirically defined as follows:

$$\alpha = \xi \frac{(v_{\mathrm{T1WM}} - v_{\mathrm{T1CSF}})^2}{8}, \tag{24}$$

where v_{T1WM} and v_{T1CSF} are the centroids of WM and CSF in T_1-weighted MR images, respectively. In general, ξ equals one. In order to investigate the influence of the parameter α on the performance of the presented segmentation method, we have selected ξ to be different values: 0.1, 0.2, 0.4, 0.6, 0.8, 1, 2, 4, 6, 8, 10 and repeated the above-noted segmentation procedure to obtain the corresponding ASR values. Figure 3 demonstrates the relationship between ξ and ASR. Over a large range of α values (where ξ value varies from 0.4 to 8), the ASR of the PV-MAP method is greater than 0.91. For all of these ξ values, the performance of the new method is better than the AFCM algorithm (which has an ASR value of 0.83).

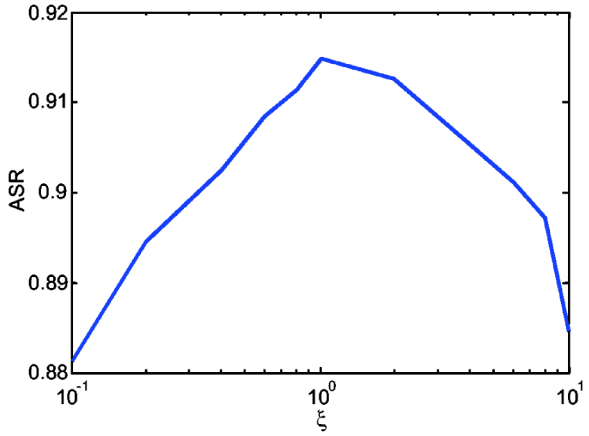

FIG. 3. Robustness study of the parameter α.

B. Clinical data studies

MRI sessions were conducted using a 1.5 T Phillip Edge whole-body scanner with a body coil as the transmitter and a birdcage head coil as the receiver. 3D SPGR and 3D EXPRESS sequences were employed to acquire T_1 and T_2 weighted axial images covering the whole brain with 30° flip angle, 1.5 mm slice thickness, 24 cm FOV, and 256×256 matrix size (0.9375 by 0.9375 mm). For the T_1 weighted image, $T_R = 50$ ms, $T_E = 5$ ms. For the T_2 weighted image, $T_R = 4000$ ms, $T_E = 95$ ms.

The self-adaptive vector quantization method[30] was used to first remove the skull and scalp and generate the initial centroids for each class. Next, the whole brain volume was segmented into three classes: WM, GM, and CSF. Figures 4(a) and 4(b) show a slice of the T_1 and T_2 weighted volume images after the preprocessing above, respectively. Figures 4(c)–4(e) show the segmentation results of the same slice using the FCM, AFCM, and PV-MAP method, respectively. It is noted that the FCM segmentation result is affected severely by the noise and inhomogeneity effect. The central WM area contains many small spots. The regions of interest indicated by the arrows near the FOV edge show the errors, which are mainly due to the inhomogeneity effect. The AFCM improved upon the results of FCM noticeably because of its correcting for the inhomogeneity effect. However, like the FCM, the AFCM is not able to overcome the noise effect, because neither of them includes the MRF model for noise control. On the other hand, the presented PV-MAP method demonstrates robustness against noise as shown in Fig. 4(e). It also achieves excellent performance in correcting for the inhomogeneity effect with the correspond-

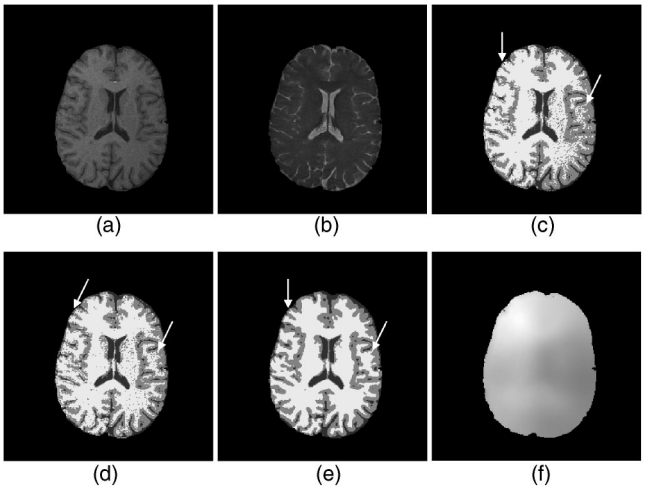

FIG. 4. Clinical study. (a) T_1 weighted image. (b) T_2 weighted image. (c) The FCM segmentation. (d) The AFCM segmentation. (e) The PV-MAP segmentation. (f) The bias field estimated by the PV-MAP segmentation method.

ing bias field estimation as shown in Fig. 4(f). Unlike the phantom studies, we do not have a gold standard for comparison in clinical studies. All of the comparisons are based on visual judgment. Most important, these experimental results concur with the theoretical predictions by the PV-MAP framework, which considers noise, PV effect, image inhomogeneity, and multispectral characteristics simultaneously.

IV. DISCUSSION

Our PV-MAP method encompasses the well-known FCM and AFCM algorithms. This can be shown from the posterior energy function U described in Eqs. (4) and (10). When α is set to zero, the proposed method reduces to the AFCM algorithm. If the bias field B is further confined to be a constant value of one, the AFCM further reduces to the FCM. The FCM reflects only the likelihood energy function in the MAP framework and the AFCM incorporates only the prior probability of the bias field B into the FCM. Neither FCM nor AFCM algorithms take into account the prior information of the mixture M, thus they fail to obtain good segmentation results for noisy MR images, which is inadequate for analysis of noisy clinic studies.

There are many ways to deal with the noise in the MR images. Edge-preserving noise filtering by an anisotropic diffusion filter (ADF) is one of many choices.[32,33] By this approach, segmenting a noisy brain MR image is performed by first smoothing the image with the ADF and then applying a previously developed segmentation method (such as the FCM or AFCM or others[34,35]) to the smoothed image. If the noise can be effectively filtered, i.e., the noise-free image can be estimated from the noisy one, most of the previous segmentation methods shall work well. To the best of our knowledge, most edge-preserving filters are suitable for the piecewise images. When there exist strong inhomogeneity or partial volume effects, the noisy images are not piecewise images anymore. The drawback of this noise-filtering and then image-segmentation approach is that a possible inconsistence of the segmented result with the original image data may occur.[36] To realize this, we performed another study. The 3D MR images with 5% noise level and different inhomogeneity effects were used. The FCM or AFCM algorithm was applied to the filtered image by the ADF. Table II shows the quantitative assessment results without inhomogeneity effect and Table III shows the results with 60% inhomogeneity effect. From these experimental results, we found that without inhomogeneity effect, FCM plus ADF approach can achieve a similar performance for noise reduction as the PV-MAP method. In the presence of inhomogeneity effect, AFCM plus ADF also showed improvement. As shown in Table I, compared with the result of AFCM algorithm, the approach of ADF filtering plus AFCM segmentation improves the ASR accuracy from 82.60% to 86.07%. However, its performance degrades in the presence of imhomogeneity effect compared with our proposed method. Therefore, the advantage of the proposed method is that it models all the effects, aiming to obtain an unbiased estimate of the noise-free signal consistent with the measured noisy data.[36]

In our PV-MAP framework, the definitions of the prior probabilities of mixture M of Eq. (5), and bias field B of Eq. (7) are not unique. For example, alternate mixture prior models for Eq. (5) were reported in Ref. 10–12. Comparing these prior models would be an interesting research topic and is under progress. For the bias field model of Eq. (7), many linear filter H can be used to model the banded covariance

TABLE III. Quantitative assessment of ADF filtering on noisy image without inhomogeneity effect (%).

	ADF+AFCM		
	WM	GM	CSF
TPF	97.15	78.67	89.16
FPF	25.53	6.59	5.50
ASR		86.07	

TABLE II. Quantitative assessment of ADF filtering on noisy image without inhomogeneity effect (%).

	FCM			PV-MAP			FCM+ADF		
	WM	GM	CSF	WM	GM	CSF	WM	GM	CSF
TPF	96.03	91.18	95.12	96.87	93.94	94.21	96.63	93.43	93.95
FPF	9.25	4.98	4.63	5.89	4.72	4.02	6.26	5.01	4.58
ASR		93.60			95.01			94.64	

matrix Σ_B in Eq. (7). Furthermore instead of using the Jacobian iterative scheme, the estimation of the bias field in Eq. (18) could be implemented by the following scheme:[23,24]

$$\beta_i = \frac{[f(Q)]_i}{[f(A)]_i}, \tag{25}$$

where f represents the low-pass filter, which corresponds to the prior model of bias field B, and Q and A were defined in Eq. (18). The Jacobian iterative scheme with multigrid strategy was employed due to its improved computational efficiency. For 3D digital MR phantom data with $181 \times 217 \times 181$ size, the total calculation time was about 10 min on a 2.4 GHz Pentium IV PC with 1 Gbyte memory. It is noted that Eq. (17) appears to be close to a discrete Poisson equation. There are highly developed analytic solutions[37] which will dramatically increase the computational efficiency for solving such equation. We will investigate the analytic solutions for an efficiency estimation of the bias field in our future work.

In this paper, the extended FCM equation was used to model the likelihood energy function $U(Y|M,B,\Phi)$ of Eq. (4). An alternative likelihood energy function could be the PV Gaussian mixture model.[10–12] One reason for choosing the extended FCM model in this paper is that the estimation of parameter Φ can be easily obtained by directly maximizing the posterior energy function as defined in Eq. (10). If the Gaussian mixture model[10–12] is considered, there are two problems that need to be solved. First, the extended Gaussian mixture model with correction of the inhomogeneity effect would need to be developed. Second, the estimation of parameter Φ for the Gaussian mixture model is not trivial and can be very difficult as compared to a conventional hard segmentation method (e.g., the MRF-EM framework[2,38]). Research on these two problems is currently under investigation by our group.[12,39]

In the work of Leemput *et al.*,[11] the PV effect was modeled by a down-sampling process, which means that PV effect comes from insufficient special resolution of the imaging devices and remains only in the boundary region between different tissues, and Monte Carlo method was used to label the subvoxels in each of the original image voxel. Their method has shown good performance of solving the PV effect. However, their method may not solve the case, in which the GM and WM are truly mixed without interfaces, as mentioned in their paper. This phenomenon occurs more often inside the tissues, which may have a pathological change, and is a very important feature for patient diagnosis. We call such segmentation as mixture segmentation, which is a more general concept than the PV segmentation. Therefore, the solution for mixture segmentation should be preformed in the continuous spaces. Accurate prior information on the mixture M is required, especially for images with more tissue types. Further investigation on this topic is one of our future research interests.[12,39]

Finally, it should be pointed out that our PV-MAP method has some limitations. The choice of weighting parameters α, λ_1, and λ_2 is empirical. In addition, the minimization algorithm used in this paper is one type of conjugate gradient method and cannot promise to converge to the global minimum, although a lot of experiments have demonstrated that it always converges to a satisfactory result. Further theoretical research is needed. The simulated annealing method or genetic algorithm may be the solution.[25]

V. CONCLUSION

A PV-MAP framework for brain MR image segmentation was proposed. The presented approach has taken into account the inherent effects of brain MR imaging including: noise, PV effect, image-intensity inhomogeneity, and multispectral characteristics simultaneously. This framework has theoretically summarized the current FCM-based segmentation methods. Digital phantom and clinical patient data studies demonstrate that this framework can improve segmentation performance over the AFCM algorithm in the presence of noise, PV effect, and intensity inhomogeneity, which are commonly encountered in clinic studies.

ACKNOWLEDGMENTS

This work was supported in part by the National Institutes of Health (Grant Nos. CA82402 and HL51466). H.L. was supported by the National Nature Science Foundation of China under Grant No. 30170278. The authors are grateful to Jennifer A. Segui for editing this paper.

[a]Author to whom correspondence should be addressed. Electronic mail: xl2112@columbia.edu

[1]M. Vannier, R. Butterfield, D. Jordon, W. Murphy, R. G. Levitt, and M. Gado, "Multi-spectral analysis of magnetic resonance images," Radiology **154**, 221–224 (1985).
[2]Z. Liang, J. R. MacFall, and D. P. Harrington, "Parameter estimation and tissue segmentation from multispectral MR images," IEEE Trans. Med. Imaging **13**, 441–449 (1994).
[3]J. C. Rajapakse, J. N. Giedd, and J. L. Rapoport, "Statistical approach to segmentation of single channel cerebral MR images," IEEE Trans. Med. Imaging **16**, 176–186 (1997).
[4]Y. Zhang, M. Brady, and S. Smith, "Segmentation of brain MR images through a hidden Markov random field model and expectation-maximization algorithm," IEEE Trans. Med. Imaging **20**, 45–57 (2001).
[5]K. V. Leemput, F. Maes, D. Vandermeulen, A. Colchester, and P. Suetens, "Automatic segmentation of multiple sclerosis lesion by model outlier detection," IEEE Trans. Med. Imaging **20**, 677–688 (2001).
[6]D. L. Pham and J. L. Prince, "An adaptive fuzzy C-means algorithm for image segmentation in the presence of intensity inhomogeneities," Pattern Recogn. Lett. **20**, 57–68 (1999).
[7]D. L. Pham and J. L. Prince, "Adaptive fuzzy segmentation of magnetic resonance images," IEEE Trans. Med. Imaging **18**, 737–752 (1999).
[8]M. N. Ahmed, S. M. Yamany, N. Mohamed, and A. A. Farag, "A modified fuzzy C-mean algorithm for bias field estimation and segmentation of MRI data," IEEE Trans. Med. Imaging **21**, 193–199 (2002).
[9]X. Li, L. Li, H. Lu, D. Chen, and Z. Liang, "Inhomogeneity correction for magnetic resonance images with fuzzy C-mean algorithm," Proc. SPIE **5032**, 995–1005 (2003).
[10]H. S. Choi, D. R. Haynor, and Y. Kim, "Partial volume tissue classification of multi-channel magnetic resonance images–A mixel model," IEEE Trans. Med. Imaging **10**, 395–407 (1991).
[11]K. V. Leemput, F. Maes, D. Vandermeulen, and P. Suetens, "A unifying framework for partial volume segmentation of brain MR images," IEEE Trans. Med. Imaging **22**, 105–119 (2003).
[12]X. Li, D. Eremina, L. Li, and Z. Liang, "Partial volume segmentation of medical images," Conference Record of IEEE NSS-MIC, in CD-ROM, 2003.

[13]L. Axel, J. Costantini, and J. Listerud, "Intensity correction in surface coil MR imaging," Am. J. Roentgenol. **148**, 418–420 (1987).
[14]T. K. F. Foo, C. E. Hayes, and Y. W. Kang, "Reduction of RF penetration effects in high field imaging," Magn. Reson. Med. **23**, 287–301 (1992).
[15]B. M. Dawant, A. P. Zijidenbos, and R. A. Margolin, "Correction of intensity variation in MR images for computer-aided tissue classification," IEEE Trans. Med. Imaging **12**, 770–781 (1993).
[16]K. O. Lim and A. Pfefferbaum, "Segmentation of MR brain images into cerebrospinal fluid and white and gray matter," J. Comput. Assist. Tomogr. **13**, 588–593 (1989).
[17]B. Johnstion, M. S. Atkins, B. Mackiewich, and M. Anderson, "Segmentation of multiple sclerosis lesions in intensity corrected multi-spectral MRI," IEEE Trans. Med. Imaging **15**, 154–169 (1996).
[18]Z. Liang, D. Wang, J. Ye, H. Li, C. Roque, and D. Harrington, "Correction of rf inhomogeneity for automatic segmentation from multi-spectral MR images," *Proceedings of the International Society of Magnetic Resonance in Medicine, 1997*, Vol. **3**, p. 2042.
[19]B. H. Brinkman, A. Manduca, and R. A. Robb, "Optimized homomorphic unsharp masking for MR grayscale inhomogeneity correction," IEEE Trans. Med. Imaging **17**, 161–171 (1998).
[20]E. A. Vokurka, N. A. Thacker, and A. Jackson, "A fast model independent method for automatic correction of intensity non-uniformity in MRI data," J. Magn. Reson Imaging **10**, 550–562 (1999).
[21]S. K. Lee and M. W. Vannier, "Post-acquisition correction of MR inhomogeneity," Magn. Reson. Med. **36**, 275–286 (1996).
[22]D. Chen, L. Li, D. Yoon, J. Lee, and Z. Liang, "A renormalization method for inhomogeneity correction of MR images," Proc. SPIE **4322**, 939–942 (2001).
[23]W. M. Wells, W. E. L. Grimson, R. Kikinis, and F. A. Jolesz, "Adaptive segmentation of MRI data," IEEE Trans. Med. Imaging **15**, 429–442 (1996).
[24]R. Guillemaud and M. Brady, "Estimating the bias field of MR images," IEEE Trans. Med. Imaging **16**, 238–251 (1998).
[25]K. Held, E. R. Kops, B. J. Krause, W. M. Wells, R. Kikinis, and H-W. Müller-Gärtner, "Markov random field segmentation of brain MR images," IEEE Trans. Med. Imaging **16**, 878–886 (1997).
[26]T. Kapur, W. E. L. Grimson, R. Kikinis, and W. M. Wells, "Enhanced spatial priors for segmentation of magnetic resonance imaging," in *Lecture Notes in Computer Science, Proceedings of Medical Image Computing and Computer-Assisted Intervention-MICCAI'98*, pp. 457–468.
[27]K. M. Pohl, W. M. Wells, A. Guimond, K. Kasai, M. E. Shenton, R. Kikinis, W. E. L. Grimson, and S. K. Warfield, "Incorporating non-rigid registration into expectation maximization algorithm to segment MR images," in *Lecture Notes in Computer Science, Proceedings of Medical Image Computing and Computer-Assisted Intervention-MICCAI'02*, pp.457–468.
[28]P. Wesseling, *An Introduction to Multigrid Methods* (Wiley, New York, 1992), p. 42.
[29]M. Unser, "Multigrid adaptive image processing," *Proceedings of IEEE Conference on Image Processing* **I**, 49–52 (1995).
[30]D. Chen, L. Li, and Z. Liang, "A self-adaptive vector quantization algorithm for MR image segmentation," *Proceedings of International Society of Magnetic Resonance in Medicine* **1**, 122 (1999).
[31]C. A. Cocosco, V. Kollokian, R. K. S. Kwan, and A. C. Evans, "BrainWeb: Online interface to a 3D MRI simulated brain database," Neuroimage **5**, S425 (1997). http://www.bic.mni.mcgill.ca/brainweb/
[32]G. Gerig, O. Kübler, R. Kikinis, and F. Jolesz, "Nonlinear anisotropic filtering of MRI data," IEEE Trans. Med. Imaging **11**, 221–232 (1992).
[33]G. Winkler *et al.*, "Noise reduction in images: Some recent edge-preserving methods," Pattern Recognition Image Analysis **9**, 749–766 (1999).
[34]X. Zeng, L. H. Staib, R. T. Schultz, and J. S. Duncan, "Segmentation and measurement of the cortex from 3-D MR images using coupled- surfaces propagation," IEEE Trans. Med. Imaging **18**, 927–937 (1999).
[35]V. Grau, A. U. J. Mewes, M. Alcañiz, R. Kikinis, and S. K. Warfield, "Improved watershed transform for medical image segmentation using prior information," IEEE Trans. Med. Imaging **23**, 447–458 (2004).
[36]J. Wang, H. Lu, T. Li, and Z. Liang, "Sinogram noise reduction for low-dose CT by statistics-based nonlinear filters," Proc. SPIE (to be published).
[37]G. Y. Hu, J. Y. Ryu, and R. F. O'Conell, "Analytical solution of the generalized discrete Poisson equation," J. Phys. A **31**, 9279–9282 (1998).
[38]A. Dempster, N. Laird, and D. Rubin, "Maximum likelihood from incomplete data via the EM algorithm," J. R. Stat. Soc. Ser. B. Methodol. **39B**, 1–38 (1977).
[39]Z. Liang, X. Li, D. Eremina, and L. Li, "An EM framework for segmentation of tissue mixtures from medical images," *Proceedings of the International Conference of IEEE Engineering in Medicine and Biology, Concun, Mexico, 2003*, pp. 682–685.